Technical Report 81
FEBRUARY, 1961

The Applicability of Seismic Refraction Soundings in Permafrost Near Thule, Greenland

U. S. ARMY
COLD REGIONS RESEARCH AND
ENGINEERING LABORATORY
Corps of Engineers

Technical Report 81
FEBRUARY, 1961

The Applicability of Seismic Refraction Soundings in Permafrost Near Thule, Greenland

by Hans Roethlisberger

U. S. ARMY COLD REGIONS RESEARCH AND ENGINEERING LABORATORY
Corps of Engineers

PREFACE

This is one of a series of reports on USA SIPRE* Project 022.01.034, Elastic and visco-elastic properties of snow and ice. The purpose of the work described in this report was to investigate the applicability of seismic refraction soundings in ice and frozen ground.

The report was written by Dr. Roethlisberger, contract scientist. T. Fohl, K. C. Thomson, R. M. Van Noy, D. White, A. A. Wickham, B. M. Hamil and other USA SIPRE and U. S. Army Engineer Research and Development Detachment personnel assisted in the field work. R. M. Van Noy and A. A. Wickham carried out most of the computations on which the results are based. U. S. Army Arctic Construction and Frost Effects Laboratory personnel provided the map of the TUTO area and carried out part of the surveying. Work on this project was performed for USA SIPRE's Basic Research Branch, Mr. J. A. Bender, chief.

This report has been reviewed and approved for publication by the Office of the Chief of Engineers, United States Army.

W. L. NUNGESSER
Colonel, Corps of Engineers
Director

Manuscript received 5 October 1960

Department of the Army Project 8-66-02-400

* Redesignated U. S. Army Cold Regions Research and Engineering Laboratory, 1 February 1961.

CONTENTS

ILLUSTRATIONS

ILLUSTRATIONS (cont.)

TABLES

SUMMARY

The applicability of the seismic refraction method for engineering purposes was investigated in the Thule area of Greenland. Special attention was given to the cases in which shallow ice overlies frozen ground and in which frozen glacial drift up to a few hundred feet thick overlies bedrock. Seismic velocities were measured in different types of sediments of the "Thule formation" and in the crystalline basement rock. The velocities in rock and frozen ground were generally high, cementation by ice being the most likely reason at the relatively low ground temperatures of about -10C. It was found that, with comparable velocity discrimination, the refraction method gives more complete information in permafrost than in unfrozen material, since later seismic events can be identified on the records shortly after the first arrival. Later events also made wide angle reflection soundings possible at a depth as shallow as 200 ft. A negative velocity gradient in the frozen ground is believed to be responsible for the rapid attenuation of the direct wave.

THE APPLICABILITY OF SEISMIC REFRACTION SOUNDINGS IN PERMAFROST NEAR THULE, GREENLAND

by

Hans Roethlisberger

INTRODUCTION

The thickness of glaciers and ice caps is usually measured by the reflection method. From a reflection survey made in 1957 on the TUTO ramp near Thule, Greenland (Fig. 1), it was learned that an ice thickness of about 200 ft is the lower limit at which reflection data can be obtained with ease (Roethlisberger, 1959). Since the glacier ends at TUTO with a gentle slope and rests on frozen till to form a thin ice body with simple surface and bottom topography, the ramp area was considered well suited for testing the refraction method on ice less than 200 ft thick. During the summer of 1958, the refraction method was tried on a portion of the ice ramp and showed good results.

A refraction survey was also carried out in the TUTO area in 1958 and 1959 to establish the thickness of the frozen till over bedrock. At the same time, velocities in a variety of rock types were measured in order to obtain more general information about the applicability of the refraction method in the Thule area and in similar formations throughout the Arctic.

GEOLOGICAL BACKGROUND AND EQUIPMENT

Geology

A thorough geological survey of the area was made recently by Davies, Krinsley, and Nicol (in press). They report various metamorphic rocks (mainly gneiss) from the Precambrian basement complex, three distinct formations of sedimentary rock, and diabase dikes and sills. Large areas are covered by glacial deposits. The sedimentary formations, formerly named the Thule formation and believed to be of late Precambrian age, are the Wolstenholme formation consisting of quartzite and sandstone; the Dundas formation consisting of black shale with some dolomite and gray sandstone; and the Narssârssuk formation subdivided into the lower red member, the Aorferneq dolomite member, and the upper red member, and consisting of red siltstone, gray dolomite, and sandstone. A cyclic repetition of sediments is typical of the lower and upper red members. Diabase dikes occur throughout the area in the crystalline basement and the sediments alike, while sills are intruded into the Dundas formation only.

Faults usually delineate the boundary between sediments and the basement rock, except in a few places where the base of the Wolstenholme formation rests unconformably on metamorphic rock. The main occurrence of the sediments is in a belt not more than 10 to 15 miles wide and extending in an east-westerly direction. Only small outcrops of the Wolstenholme formation are located south of the southern limit of the sedimentary belt. Although the faults follow an east-west trend, they may not be extrapolated very far under glacial deposits or the ice cap because they are not straight and form a complex system.

The surficial deposits consist mainly of boulder fields, moraine, outwash, and talus of varying thickness. In many places in and around Thule Air Base special information of an engineering nature has been gathered on surficial deposits by different agencies. Hvorslev and Goode (1960) have described cores to a depth of 63 ft in coarse glacial till at TUTO. These consisted of silty sandy gravel with numerous cobbles and boulders but relatively little ice. A water content between 5 and 10% of dry weight was usually found.

Permafrost temperatures

Temperature information was obtained from a 1000 ft deep drill hole in bedrock near Thule Air Base (ACFEL files). A temperature of -4.3C was reported from 1002 ft depth and a gradient of 0.7C per 100 ft was found between 500 and 1000 ft. Extrapolation gives -11C at 50 ft, 0C at 1600 ft depth. The temperatures above 500 ft seemed to be too much affected by the air temperature during drilling to be of any use.

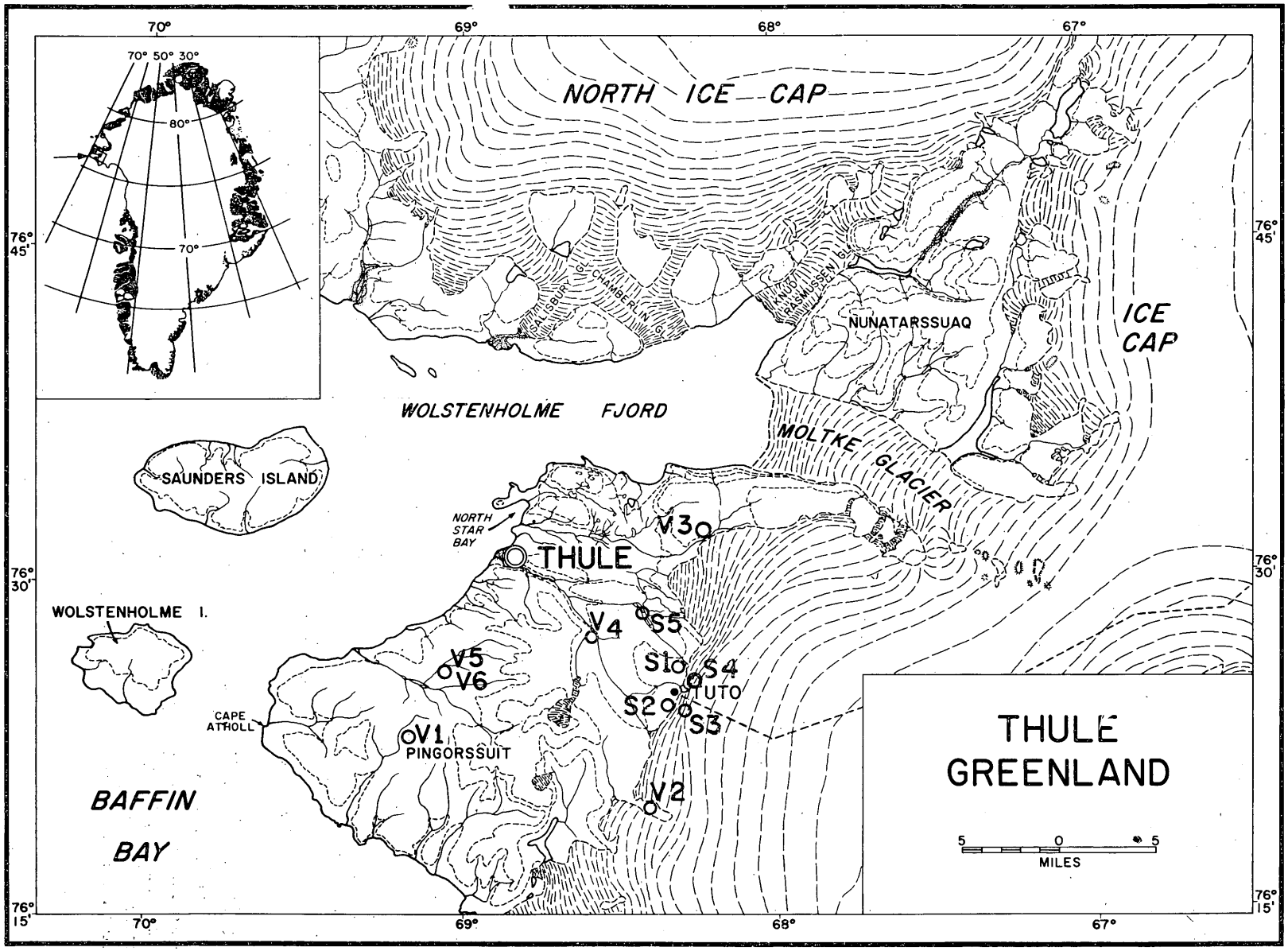

Figure 1. Thule area where velocity measurements (V) and soundings (S) were made.

The temperature profiles presented by Hvorslev and Goode (1960) give -12C at 50 ft depth with a seasonal change of less than 1C. (For temperatures at different times of the year see ibid., Fig. 5) They report a temperature of about -11C in ice near the edge of the ice cap.

Equipment

The seismic equipment used for both reflection and refraction soundings was a high frequency system, model P-15 with accessories, manufactured by the Southwestern Industrial Electronics Company (SIE). The geophones, SIE type S-16, have a natural frequency of 18 cps, with damping 0.56 of critical. The amplifiers are equipped with automatic gain control, suppression, filters and mixing circuits. No suppression was applied throughout the survey. The filters were generally set for the band between 70 and 425 cps or 220 and 425 cps. The explosions were fired by a capacitor blaster, SIE type PC B-11, using Atlas "Staticmaster" caps. Military explosive Composition C-4 or 60% dynamite was used.

Nine channels were used in 1958, 12 in 1959. In some instances two seismic cables were used to stretch the geophone line. Unfortunately, the outlets were numbered in reverse order on one cable, with the result that some traces are out of order on the records, as in Figures 10 and 11.

VELOCITY MEASUREMENTS

Objective

The refraction technique can be successfully applied only when a lower velocity material occurs over a higher velocity refractor. Thus the velocities of the materials must be known for proper planning of a refraction survey. Again, the velocities must be known if identification of an unknown refractor is to be attempted. Since the Thule area is quite complex geologically, a special effort was made to determine velocities in different formations.

Technique

Weathering sometimes makes it difficult to measure accurately the velocity of elastic waves (seismic velocity) on rock outcrops. Not only is the velocity changed in the weathered zone, but also the frequency of the first break often becomes so low that accurate measurements over a short path are impossible. However, in cold regions where the permafrost is well developed, the weathering zone is very shallow and it is much easier to make reliable velocity measurements at the surface. It was found that the following method furnished the best results with the least effort.

A flat surface was chosen close to an outcrop — so that there was no doubt about the exact nature of the bedrock — but where the rock was covered with a thin and most probably uniform layer of topsoil and the surface showed frost pattern features. The topsoil consisted of heterogeneous glacial drift or decomposed debris of the underlying bedrock. A row of geophones was laid out with approximately equal spacing and in as nearly a straight line as possible, considering the necessity of locating each geophone on a patch of fine material (center of fines) in the frost pattern. The arbitrary distance between geophones was about 50 or 100 ft. The explosive charges were placed close to both ends of the line, also in centers of fines. If conditions permitted, additional charges were set off at greater distances up to several hundred feet from either end of the geophone line. A hole was dug to the frost table or a crater was blasted with a preliminary charge so that the explosives were always in contact with the frozen ground. For 500 ft lines, about 2 lb of 60% dynamite was used.

Since in this method neither geophone nor shot point is placed on the bedrock to be investigated, but rather on a low-velocity top layer, use is made of refracted waves which are affected by thickness and velocity of the low-velocity layers. Nevertheless, the scatter of individual points around a straight time-distance curve was less than

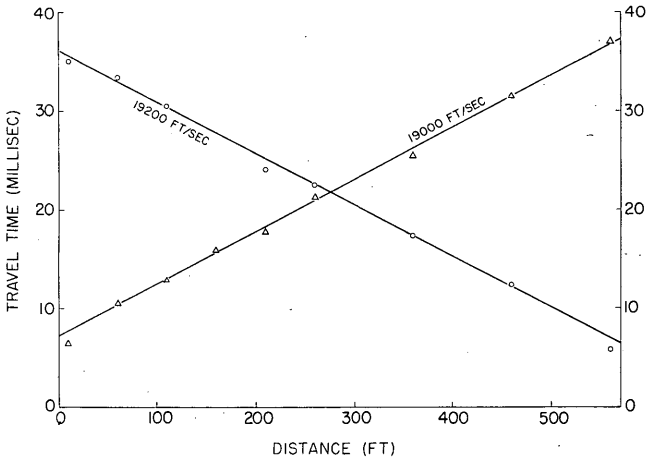

Figure 2. Time-distance curves of a velocity profile on a dolomite plateau, V4.

when the geophones were placed on exposed bedrock and direct waves were measured. The exposed rock is probably slabbed off and invisibly shattered by frost, which could account for scatter in the direct-velocity measurements. The small scatter in the refraction arrivals indicates amazingly homogeneous conditions in the low-velocity layers as well as undisturbed rock underneath. Some features of the permanently frozen ground and the seasonally thawing and freezing active layer on top may explain this.

Permafrost may consist of debris or jointed rock cemented by ice and is normally impermeable to water. Physically speaking, most types of permafrost may be considered as massive rock. Because of thermal contraction in winter, this massive rock will crack from the surface down to a limited depth in a polygonal pattern, but these cracks will heal when they fill with melt water in early summer or thermal expansion closes them again as seasonal heat penetrates downward. Only the ice wedges developing in the cracks and growing over the years need be considered in velocity studies. This is the only weathering process in the permafrost zone.

In the active layer where excess weathering takes place, the conditions are also rather simple. The active layer is of very limited thickness, usually between 3 and 7 feet in the Thule area, but cannot be neglected because of the small velocities. One of its outstanding features is the sorting of particles of different size. A vertical sorting, in which the coarse particles move to the top, can be distinguished from a horizontal sorting, in which they move away from centers of fines and accumulate in patches and rows to form a sorted net pattern. On a slope, lines of coarse material alternate with stripes of fines. The fines were chosen as bases for both the geophones and the charges because the findings of Corte (personal communication) indicate the fines to be better locations than accumulations of coarse debris or areas of little sorting. The important features of the centers of fines and stripes are:

1. Greater homogeneity over the full thickness of the active layer.
2. Less penetration of thawing, i.e., a thin active layer.
3. Retention of moisture, assuring good transmission of the elastic waves.

No detailed study of the low-velocity layers was carried out. However, it can be stated that the total effect, i.e., the vertical shift of the time-distance curve (intercept time), varied between 2 and 10 milliseconds. Individual points were seldom more than one millisecond in error. A typical example of a time-distance graph is given in Figure 2. The frequencies of the first few cycles on the records varied between 200 and 500 cps. The frequency bands of the equipment were set for a range of either 70 to 425 cps or 220 to 425 cps.

Results

Presentation of data. For velocity measurements the paper speed of the recorder was usually set at 4 ft/sec. Lengths on the records were measured with a millimeter scale, estimating to tenths of a millimeter, which corresponds approximately to tenths of a millisecond. Time intervals were determined to both the first break and the first peak unless one of these features was of bad quality or missing. Zero time was usually taken at the time break signal from the blast, with no cap-delay correction applied.

The first break of the first geophone or an arbitrary time line was taken as zero when the time-break signal was missing. The "travel time" thus determined was plotted against distance from the first geophone or the shot point and the points which were part of the straight refraction branch were determined from the graph (Fig. 2). Quite often the first geophone could not be used because its first arrival belonged to a wave which did not reach the bedrock being investigated. Whether the zero time of the blast was known or an arbitrary zero had to be used is unimportant, since the thickness of the surface layers was not of interest and the velocity is computed only from the slope of the time-distance graph. It can be seen from the travel-time data (App. A) whether true or relative travel times are stated.

After excluding the points not part of a straight line (marked with asterisks in Appendix A), the travel-time data were processed by a standard linear regression program on an electronic Bendix G 15 D computer and the velocities found as the reciprocal of the slope of the regression line (reciprocal regression coefficient). The results are presented in Table I. The first three columns are self-explanatory. Column 4 gives an identification number referring to Appendix A and column 5 indicates whether the first breaks or first peaks were used to determine the travel time. Columns 6 and 7 give the velocities as computed from the regression coefficient. The standard deviation σ_c from the regression line (col. 8) is defined by the equation

$$\sigma_c = \sqrt{\frac{\Sigma (y_i - Y_i)^2}{N - 2}}$$

with y_i = measured value and Y_i = calculated value of y for argument x_i; N = number of measurements; and i = 1, 2, 3 ... N. The standard error p_v of the velocity (col. 9) is defined by

$$p_v = \frac{100\ \sigma_c}{b\sqrt{\Sigma (x_i - \bar{x})^2}}$$

with b = slope of regression line, $\bar{x} = \Sigma x/N$. A mean velocity value was computed for each rock type by taking the reciprocal of the arithmetic mean of the slopes (col. 10, 11). Column 12 gives the deviation of the individual velocities from the mean value. The mean velocity and the deviations from it do not have much statistical value because individual velocities were not systematically sampled and are sometimes dependent on each other when the same data were used in more than one regression calculation.

Columns 8, 9 and 12 provide information on the accuracy of the velocity survey. The standard deviation of the measurements from the straight regression line is frequently smaller than 0.5 and seldom more than 1.5 millisec. The larger part of this scatter is probably due to inhomogeneities at the geophone locations. The standard error of the individual velocity determinations p_v (col. 9) was usually found to be from 1 to 3 %. In some cases where results from shots at different distances and/or from more than one line were available, the deviation from the mean velocity value (col. 12) appears to be larger than might be expected from the standard error p_v. Inhomogeneity of the rock is probably the reason for this. A change of velocity by a small percentage can be considered normal for most rock formations.

Improved method of computing velocities. Part of the standard deviation σ_c is caused by inhomogeneities at the geophone locations. In particular, the thickness of the low-velocity surface layer (the depth to the frost table) may change from one place to another, as well as the velocity within this layer. In these cases the refracted signals at one specific geophone are affected by about the same amount, and the travel times from the two directions of shooting will both be either too short or too long by approximately the same amount. An example of too-short travel-times may be seen at the fifth geophone from the left in Figure 2. This type of scatter can be cancelled out if the differences Δ between travel times from the two shots are used to determine the velocity rather than the travel times proper. The time differences versus the distance are expressed by a straight line with slope b_Δ. The

Table I. Velocity measurements in the Thule area.

1 Location	2 Formation	3 Rock type	4 Regression no.	5 Signal type	6 Velocity (ft/sec)	7 Velocity (m/sec)	8 σ_c (millisec)	9 p_v (%)	10 Mean velocity (ft/sec)	11 Mean velocity (m/sec)	12 Deviation from mean (%)
V 1	basement rock	gneiss	42	break	21,398	6522	0.74	4.52	19,961	6084	+ 7.19
			43	break	20,188	6153	0.26	1.33			+ 1.13
			44	peak	19,108	5824	0.37	2.16			- 4.27
			45	peak	19,310	5886	0.66	3.95			- 3.26
V 2	Wolstenholme	quartzite	34	break	18,499	5640	0.41	1.19	18,891	5758	- 2.08
			35	break	18,820	5738	0.40	1.28			- 0.38
			36	break	19,355	5901	0.57	1.89			+ 1.93
V 3	Dundas	black shale	11	break	13,422	4092	0.63	1.88	13,379	4078	+ 0.32
			12	break	12,710	3875	0.52	1.39			- 5.00
			13	peak	12,582	3836	0.61	1.60			- 5.95
			14	break	13,366	4075	0.84	1.89			+ 0.10
			15	peak	13,704	4178	0.78	1.80			+ 2.43
			16	break	13,963	4257	0.81	1.90			+ 4.37
			17	break	13,596	4145	1.51	2.11			+ 1.62
			18	peak	13,796	4206	1.51	2.25			+ 3.12
		grey sandy shale	19	break	13,605	4148	1.09	2.50	13,996	4266	- 2.80
			20	peak	14,416	4395	0.61	2.27			+ 2.99
V 4	Narssârssuk	dolomite	3	break	19,498	5943	0.36	1.38	19,341	5895	+ 0.82
			4	peak	19,713	6009	0.50	1.96			+ 1.93
			5	break	18,983	5786	0.44	1.81			- 1.84
			6	peak	19,180	5846	0.49	2.71			- 0.82
V 5	Narssârssuk	sandstone	37	break	16,190	4935	0.65	2.73	16,539	5041	- 2.12
			37.1	break	15,670	4776	0.76	2.18			- 5.26
			38	peak	16,753	5106	0.86	4.45			+ 1.29
			38.1	peak	15,753	4802	1.46	5.64			- 4.75
			39	break	17,878	5449	0.68	3.13			+ 7.99
			40	break	17,036	5193	0.92	4.03			+ 2.99
			41	peak	16,713	5094	0.74	3.21			+ 1.05
V 6	dike	diabase	7	break	18,832	5740	0.58	2.82	18,107	5519	+ 4.00
			8	peak	17,888	5452	0.40	2.22			- 1.21
			9	break	17,730	5404	0.34	1.54			- 2.08
			10	peak	18,018	5492	0.29	1.59			- 0.49
S 1	glacial deposit	till	21	break	15,493	4722	0.17	0.91	15,469	4715	+ 0.16
			24	break	15,444	4707	0.25	1.97			- 0.16
S 5	glacial deposit	outwash	25	break	14,671	4473	0.42	1.25	14,675	4473	- 0.03
			26	peak	14,462	4409	0.50	1.47			- 1.45
			27	break	14,193	4327	1.11	2.66			- 3.28
			28	peak	14,094	4297	0.96	2.29			- 3.96
			29	peak	14,809	4515	0.33	0.93			+ 0.91
			32	break	15,308	4667	0.46	1.20			+ 4.31
			33	peak	15,222	4641	0.38	0.97			+ 3.73
Petowik Glacier	glacier ice	ice	0	break	12,143	3701	1.54	1.24	12,178	3712	- 0.29
			1	break	12,237	3730	1.10	0.63			+ 0.48
			2	break	12,155	3705	1.11	0.90			- 0.19

Table II. Velocities determined by eq. 1.

Location	Rock type	Regression no.	Signal type	Velocity ft/sec	Velocity m/sec	σ_c (millisec)	p_v %
V 1	gneiss	111	peak	19,062	5810	0.88	3.15
V 2	quartzite	103	break	18,481	5633	0.12	0.19
V 3	black shale	106	break	13,199	4023	0.39	0.54
"	" "	107	peak	13,330	4063	0.36	0.50
V 4	dolomite	101	break	19,190	5849	0.42	1.20
"	"	102	peak	19,213	5856	0.50	1.39
V 5	sandstone	110	break	17,395	5302	1.11	2.45
V 6	diabase	104	break	18,264	5567	0.63	1.50
V 6	"	105	peak	18,110	5520	0.27	0.92
S 5	outwash	108	break	14,747	4495	1.11	1.31
"	"	109	peak	14,639	4462	0.99	1.23

velocity $\underline{v}$ then is found from

$$v = 2/b_\Delta . \qquad (1)$$

Eq 1 only holds when the frost table, assumed now to be planar for the length of the profile, is parallel to the surface, i.e., when the two velocities v_+ and v_- determined from the two directions of shooting are equal. If the frost table forms an angle θ to the surface (in the plane of the profile), then b_Δ is related to v_+ and v_- by

$$b_\Delta = \frac{v_+ + v_-}{v_+ v_-} ,$$

and the true velocity $\underline{v}$ is found from

$$v = 2 \cos\theta / b_\Delta . \qquad (2)$$

Eq 1 and 2 differ by the factor of $\cos\theta$, where the angle is not known. In order to compute θ from seismic data, the velocity in the surface layer must be determined. However, since the active layer, as the low-velocity surface layer, cannot change much in thickness, θ can only be very small, and eq 2 is sufficiently approximated by eq 1. For $\theta = 2.5°$, the result would be only 1/10% too small, and 1% for $\theta = 8°$; the angle θ could hardly ever reach 1° for a 500 ft long profile.

The possibility must also be considered that the second side of the angle θ may be formed by the top of the bedrock rather than the frost table. In this case a wedge-shaped intermediate body of frozen ground of gradually changing thickness exists between the frost table and the top of the bedrock. As will be shown the velocity in such material is comparatively high, only about 10 to 30% smaller than the bedrock velocity. No reason exists for θ to be small in this case; however, the difference between v_+ and v_- will increase with increasing θ. If this difference is found to be greater than 5 to 10%, the result from eq 1 should be tested, using eq 2 with appropriate assumptions. For shots close to the end geophones, the presence of the wedge-shaped intermediate velocity body would be obvious because of a break in the time distance curve, at least in one direction.

A number of velocity profiles were analyzed using eq 1, computing b_Δ by least squares from the individual values of Δ stated in appendix B, and the results are presented in Table II. The improvement achieved is best expressed in the standard error p_v of the velocity, which is somewhat smaller in Table II than in Table I. To get a clearer picture of the improvement, corresponding p_v-values from the two tables must be compared, as shown in Table III. Only the values with asterisks were obtained from the same geophones (comparable statistical samples). In the other cases, the regression of the single-direction time-distance curve was computed with more values than the two-direction combination. In only two cases did the latter show larger errors than one of the single-direction curves; in most cases a considerable improvement was achieved.

Table III. Comparison of standard error of velocity.

Regression no.	Compared with regression no.	Improvement of p_v (difference in %)	
111	44, 45	-0.99	0.80
103	34, 35	1.00	1.09*
106	12, 14	0.85*	1.35
107	13, 15	1.10*	1.30
101	3, 5	0.18	0.61
102	4, 6	0.57	1.32*
110	39, 40	0.68*	1.58*
104	7, 9	1.32*	0.04*
105	8, 10	1.30	0.67
108	25, 27	-0.06*	1.35*
109	26, 28	0.24*	1.06*

Table IV. Comparison of velocities determined from breaks and peaks.

Regression no.	v(pk)-v(bk) (ft/sec)	σ_c(pk)-σ_c(bk) (millisec)
12, 13	-128	+0.09
14, 15	+338	-0.06
40, 41	-329	-0.45
25, 26	-210	+0.08
27, 28	- 98	-0.15
32, 33	- 85	-0.08

Table V. Velocities determined from the time-distance graphs.

Location	Formation	Rock type	Velocity (ft/sec)		Velocity (m/sec)	
V 1	Basement rock	Gneiss	20400	± 400	6220	± 120
V 2	Wolstenholme	Quartzite	18700	± 300	5700	± 90
V 3	Dundas	Black shale	13000-14000	± 500	3960-4260	± 150
"	"	Sandy shale	14500	± 500	4420	± 150
V 4	Narssârssuk	Dolomite	19100	± 200	5820	± 60
V 5	"	Sandstone	17200	± 200	5240	± 60
V 6	Dike	Diabase	(18500 ?	± 500)	(5640 ?	± 150)
S 1, 2, 3	Glacial deposit	Till	15700	± 300	4780	± 90
S 5	"	Outwash	15200	± 300	4630	± 90
S 2	Glacier	Ice	12200	± 500	3720	± 150

Comparison of measurements from first breaks and first peaks. In a few cases both the first break and the first peak were used from the same traces on a record. The results are compared in Table IV. With one exception, there seems to be a tendency to slightly lower velocities from the peaks than from the breaks, which means that the frequency of the first wave train decreases sufficiently with distance to affect velocity measurements. This effect, however, is in the same order of magnitude as the standard error of the velocity and may, as a rule, be neglected. The standard deviations from the straight line, also compared in Table IV, are not significantly different for the two methods. It is readily apparent, therefore, that first breaks and first peaks can be used equally well for a velocity survey.

Graphical velocity determination. Before the regression analysis was carried out, velocities were determined graphically from the time-distance graphs. Approximate mean velocities obtained in this way are stated in Table V. The estimated error is not a defined figure, but rather an indication of the accuracy assumed to have been

achieved, taking into account the differences found between two directions of shooting in a profile, between close-up and more distant shots, and between different profiles if more than one were located in the same material.

Comparison of tables V, I, and II suggests that there was a tendency to draw the time-distance lines too flat in the graphical analysis and to underestimate the error. The general agreement, however, is good and for most practical purposes the much faster graphical method works satisfactorily.

Discussion of the velocity values. No attempt has been made to correlate the velocity values with petrological data. However, since representative outcrops for the several formations were chosen, general information on the nature of the rocks may be obtained from the geological literature (Davies et al.). The relatively low velocity in diabase cannot be accepted as representative. Since the measurements were made close to the edge of a cliff along a low ridge formed by the dike, it is likely that the cracks in the generally shattered diabase do not contain much ice or that the shattering was extreme.

The other rocks show high velocities throughout for the material, probably because of cementation by ice. That ice is a good rock cement is illustrated by the high velocities found in glacial deposits. The till consists of boulders, cobbles, and pebbles in a matrix of sand and silt. The outwash shows only cobbles and pebbles at the surface, but sand and silt are also present in deeper layers according to a drill log. It is noteworthy that the velocity in these frozen glacial deposits is clearly higher than in the shale of the Dundas formation.

As a hypothesis, one can assume that the velocity in frozen ground and shale will depend primarily on the amount of air, ice, and clay minerals present. When ice fills an air space and acts as a cement, the velocity increases. When it becomes abundant enough to be an important fraction of the ground, the velocity is bound to decrease, because the velocity is lower in ice than in most rock fragments. Furthermore, the velocity in a mixed substance can be lower than in either one of the components. Clay minerals in a soil below 0C cause a low velocity since water adsorbed by them will not be completely frozen. The amount of unfrozen water will depend on the temperature; hence velocity will have a considerable temperature dependence in rocks containing clay minerals. Around Thule and TUTO ground temperatures of -10C to -12C have been reported at 30 to 50 ft depth, i.e. below the zone of significant seasonal variation. From the Fairbanks district of Alaska, where the ground temperatures are considerably closer to 0C, Joesting (1954) reports velocities of 13000 to 15250 ft/sec in frozen gravel and 250 to 10000 ft/sec in frozen muck. The former values are comparable to the velocities in frozen outwash shown in Table I; the latter ones are smaller than any value in this table. Unfrozen old till with some cementation shows velocities up to a little over 9000 ft/sec according to Linehan (1951).

During the summer, when these measurements were carried out, there is a negative temperature gradient with depth at the top of the permafrost. Velocity should therefore increase with depth, and the velocity should increase with distance from the shot point, i.e., the time-distance curve should be convex in the direction of the ordinate. No such curvature was apparent in the graphs, but in the cases where shots were fired at more than one distance, the more distant shot usually gave a slightly higher velocity than the less distant one. In the profile on Wolstenholme quartzite a velocity of v = 18,820 ft/sec (5738 m/sec) was found for a shot at 88 ft from the first geophone, as against v = 19,355 ft/sec (5901 m/sec) for a shot at 510 ft (regressions 35 and 36). Similar effects were observed in shale and outwash. The magnitude of the effect is compatible with a positive velocity gradient down to a few meters.

SOUNDINGS

Objectives

The refraction soundings were primarily experimental, to determine if and where the method could be applied successfully. The locations are shown in Figures 1 and 3. Only the cases of ice over glacial deposits; glacial deposits over bedrock; and the three-

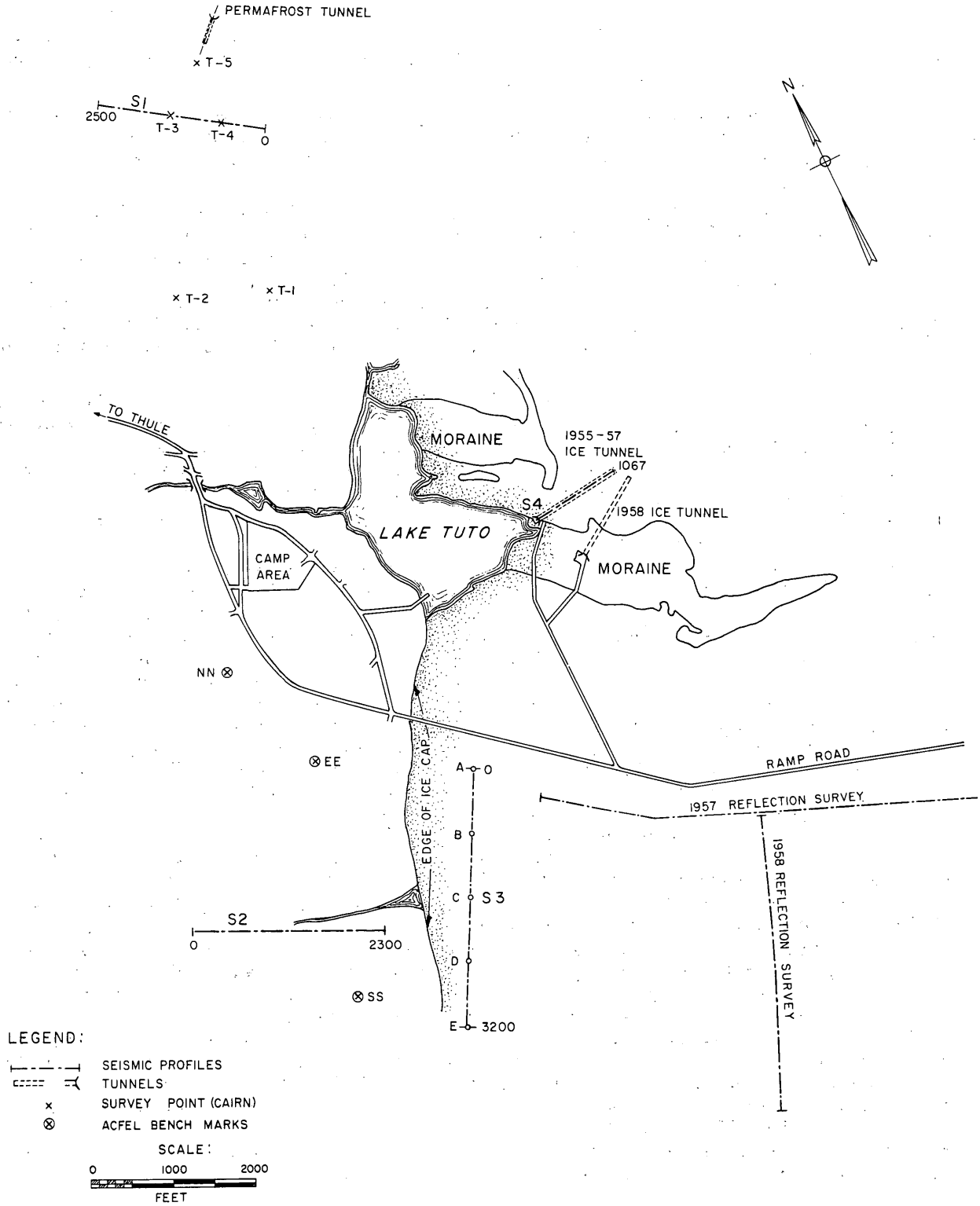

Figure 3. Detailed map of the vicinity of Camp TUTO. (Based on field sketch provided by USA ACFEL personnel).

layer case with ice, till, and high-velocity bedrock were examined. Some of the results were of morphological significance and some had an engineering application.

Technique

On the glacial deposit, the same set-up was used as for the velocity measurements, i.e., the geophones and charges were placed on centers of fines with the charges at the frost table. The geophones, spaced 100 to 250 ft apart, were left in place and the shot points moved out along a straight line until the high velocity showed up in the first arrivals. The geophones were then moved to the opposite end of the profile and the shots were fired from the side of the profile where the geophones had been before. The procedure was similar on the ice cap with geophones and shots placed at the surface of the ice. The geophones were buried slightly in the ice and covered with a pile of ice chips to prevent them from thawing into the ice and being supported by the rubber cap instead of the base.

The longest profile on frozen ground was 2800 ft, for which 12 1/2 lb of high explosive was used at the end shot points. On the ice, the same amount of explosive was used for 3200 ft. Later in the survey it was learned that low-amplitude records furnished information on later arrivals and after that every shot was fired twice, once with a large charge for first breaks, once with a lesser charge for later arrivals.

Results

Applicability. A general indication of the applicability of the refraction method can be obtained from the velocity tables. There are a number of formations with velocities distinctly different from each other, which means that the refraction method will work if the lower velocity formation is on top. This will generally be the case, since the succession of ice, glacial deposit, sedimentary rock, and basement rock show successively higher velocities, with the exception of shale underlying glacial deposits. Since the differences in velocities are not large, long profiles are required relative to the depth to be measured and relatively low accuracy of the results is inherent.

TUTO terrace (S1, S2). Camp TUTO is located on a terrace which extends for about 2 miles along the edge of the ice cap and is roughly 1/3 mile wide. The ground consists of glacial drift, mainly coarse till. No bedrock outcrops occur closer than 3 miles from TUTO, which makes it impossible to estimate the thickness of the glacial drift from geological features. The deepest drill hole made so far was sunk some 70 feet into frozen till without reaching bedrock. The nature of the bedrock under TUTO is equally uncertain, since the main fault separating the sediments from the basement rock trends toward TUTO and may as well be located north, south, or directly under the terrace.

The primary objective of seismic soundings on the TUTO terrace was to ensure the existence of sufficient glacial drift at the site of the permafrost tunnel. The survey was only carried as far as necessary for this purpose, and no special effort has been made to achieve high accuracy or to determine the nature of the bedrock. The results obtained are thus not indicative of the ultimate possibilities of the seismic method.

The time-distance graph and the interpretation for the profile at S1 are given in Figure 4; the individual travel times obtained from the records are given in Appendix C. With a velocity of 16000 ft/sec in the frozen till and 22000 ft/sec in the bedrock, the depth of the interface is found to be 410 ft (solid line). Merely changing the velocity gives a lower limit of 325 ft and an upper limit of 510 ft (dashed lines). Assumptions for the presence of additional layers are expressed in the 2nd and 3rd column of Figure 5, the 1st column representing the simple two-layer case of Figure 4. A fourth assumption, the presence of a sediment which might begin at any depth down to the high-velocity layer, and with a velocity equal to that of the till, cannot completely be ruled out. However, such a sediment would be soft and unlikely to exist on top of a hill. The high-velocity bedrock is likely to be gneiss, but other rock types could be considered with the limited information on velocity available from Figure 4.

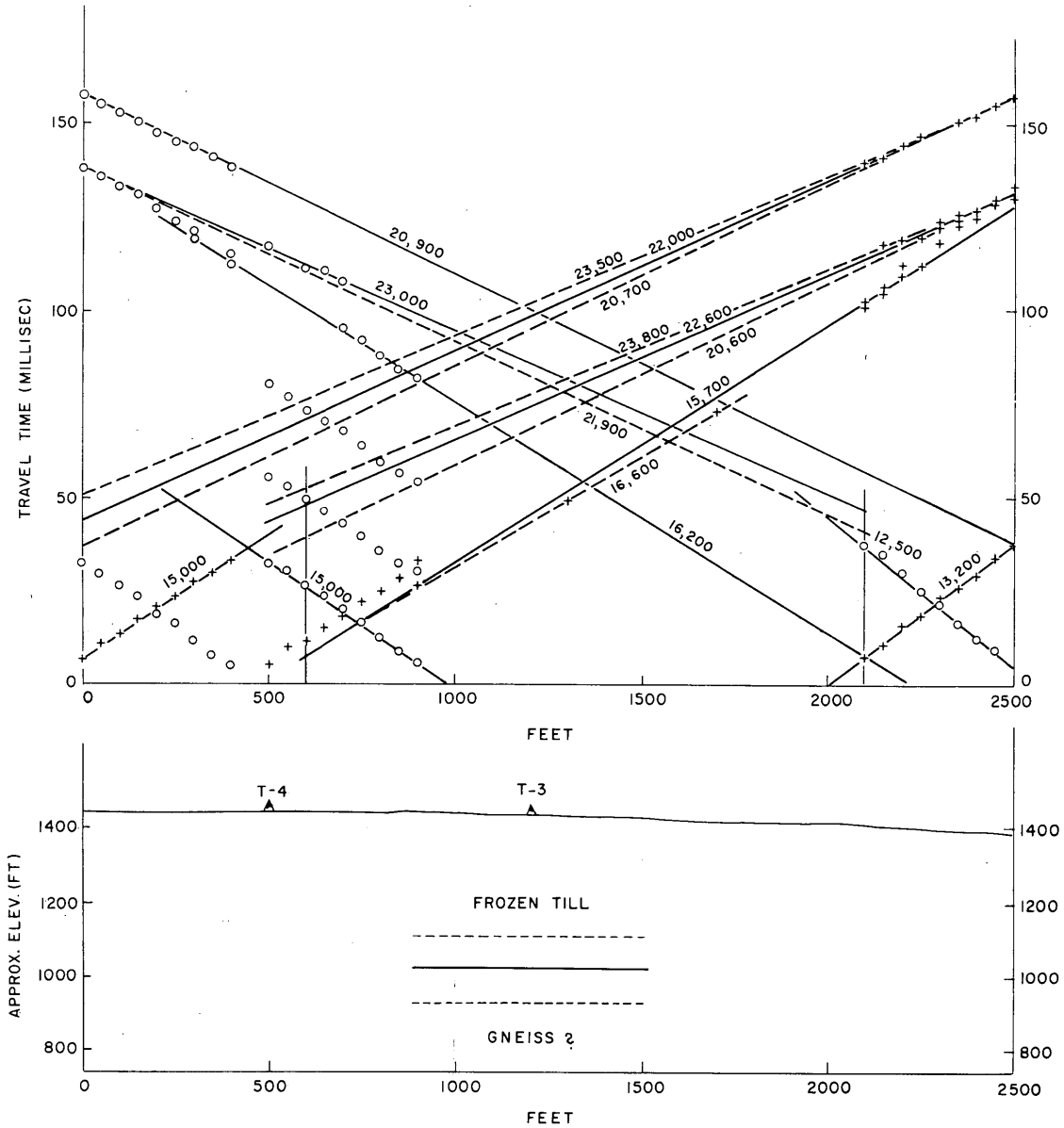

Figure 4. Time-distance curves from soundings on the TUTO terrace at S1. Solid and dashed lines represent most probable and extreme assumptions respectively. Below, cross section through survey points T-3 and T-4.

A similar profile (S2) was surveyed near the southern end of the terrace with almost identical results (Fig. 6). Individual data are tabulated in Appendix C. The most probable figure for the depth to the interface here is 400 ft if only till and high-velocity bedrock, presumably gneiss, are assumed to be present. The consistency of the 400 ft depth is in favor of this simplest case, because the more complex the stratigraphic section, the less likely conditions are to be identical over a large area. The same argument can be used against complicated geometry in the two-layer case.

It can be concluded with a high degree of confidence that the glacial drift is several hundred feet thick below the surface of the TUTO terrace, most probably about 400 ft.

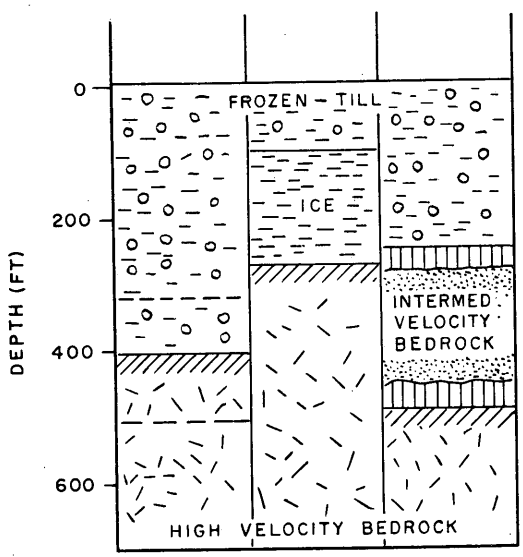

Figure 5. Alternative interpretations of profile S1.

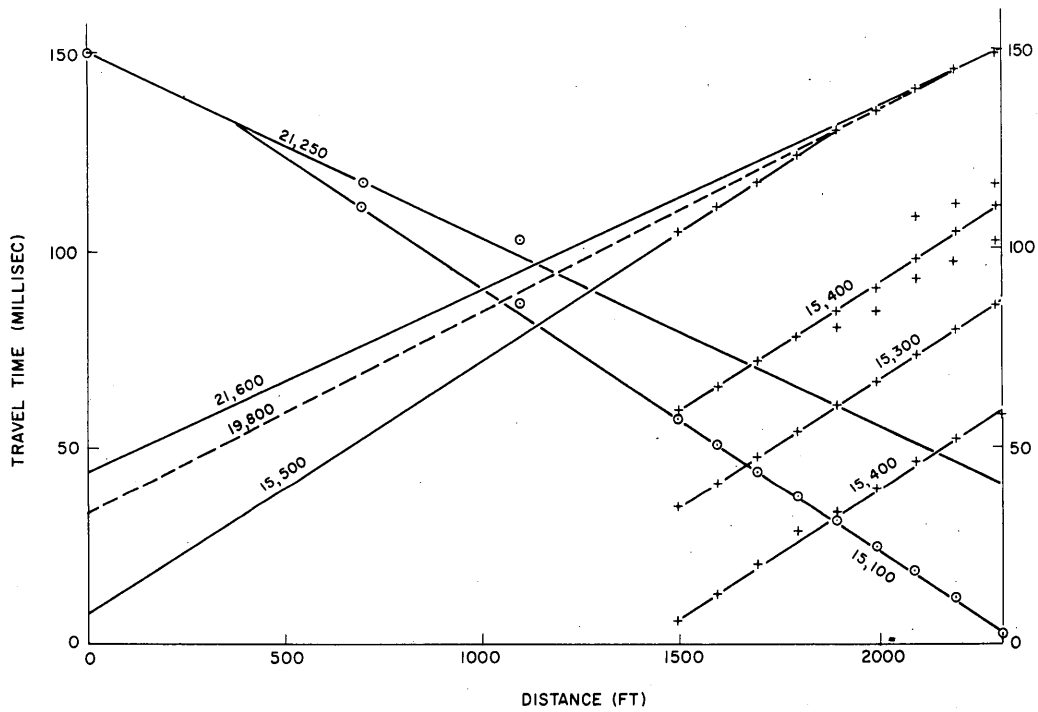

Figure 6. Time-distance curves from soundings at S2 on the TUTO terrace.

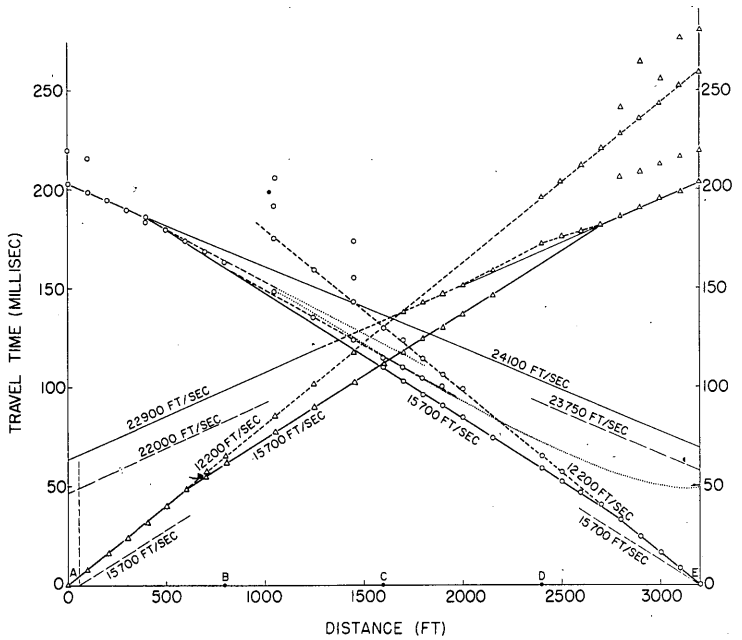

Figure 7. Time-distance curves from soundings through ice and frozen ground to bedrock at S3. Light solid and dashed lines show first approximation with topographic and top-layer corrections. Heavy dashed and dotted lines show alternative and more elaborate interpretations.

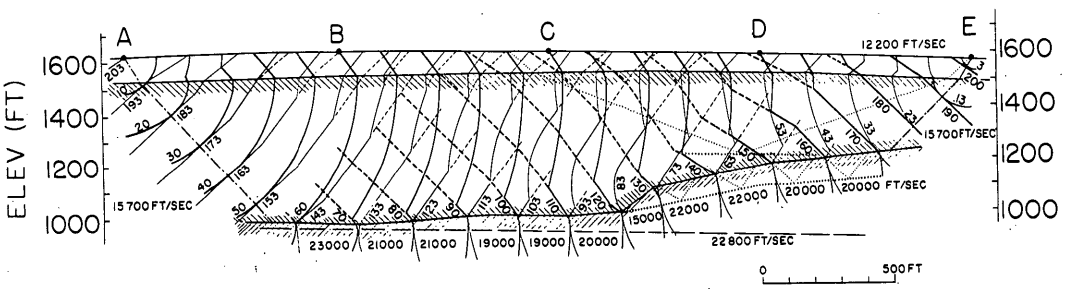

Figure 8. Pairs of wave fronts originating at A and E and the results of soundings at S3. The solid, dotted, and light dashed interfaces represent different interpretations of the time-distance curves in Figure 7.

Edge of ice cap (S3). A refraction profile 3200 ft long was established at location S3 on the ice cap close to its edge. The travel time data are given in Appendix C for all five shot points and all three geophone spreads. The travel time curves for the end shot points A and E of all spreads are plotted in Figure 7. In Figure 8 the corresponding cross section containing interfaces and wave fronts is presented. The ice thickness at B, C and D was found from travel time curves of the pertinent shots not plotted in Figure 7. The refraction method proved adequate to measure the small ice thickness of the profile, which varied between 75 and 100 ft. There is no doubt that the underlying material is till, as reflected by a velocity of about 15700 ft/sec in the refraction profiles.

Strong signals from a high velocity refractor could be obtained as first and later events. By using the first arrivals mainly, apparent velocities of 22900 ft/sec and 24100 ft/sec respectively can be determined from the last branches of the time-distance curve for shot points A and E. The velocities are reduced somewhat when the top

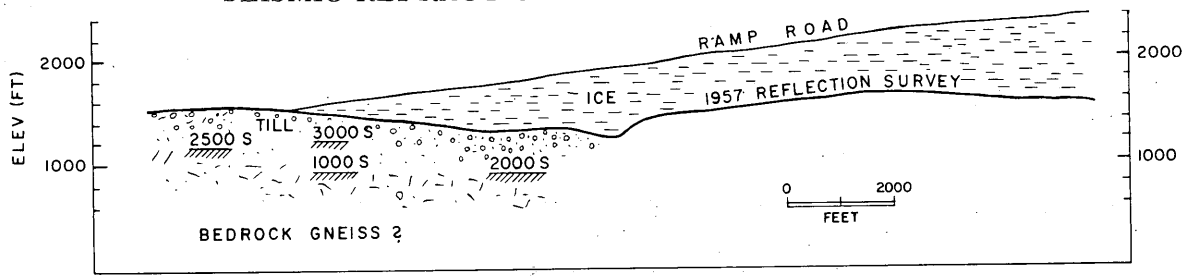

Figure 9. Cross section perpendicular to the edge of the ice cap, south of the ramp road.

layer is eliminated and the topographic correction is applied, and a velocity of 22400 ft/sec is found for the refractor at a depth of approximately 600 ft below the surface of the till. Travel-time curves reduced for top layer and topography and the corresponding interface are shown by long dashed lines in Figures 7 and 8.

A flat interface (straight last branch in the time-distance curve), however, does not take into consideration some of the later events at shorter distances, and also the velocity found is too high compared to the values from the adjacent TUTO terrace. A more detailed cross section was therefore constructed (Fig. 8) using the wavefront method (Hagedoorn 1959, Thornburgh 1930). In both Figures 7 and 8, solid lines are used for first arrivals, short dashed lines for later events. The dotted lines refer to a different assumption interpreting part of the later events as reflection signals from an intermediate reflecting surface.

The wavefront method gives a relief more complex than that of a plane for the surface of the refractor, which also shows a low velocity, averaging 20000 to 21000 ft/sec. This value may suggest that the refractor consists of gneiss. However, at least part of the velocity variation in the refractor found with the wavefront method may be due to inaccuracy inherent in the data.

The results at S2, S3 and a refraction sounding carried out in connection with reflection studies further up the ramp (1958) are plotted in Figure 9, which also shows the 1957 ramp road profile (Roethlisberger, 1959, Fig. 3). The numbers followed by S in the graph give the approximate distance in feet south of the plane of this profile.

Old ice tunnel (S4). During the 1957 seismic survey, refraction signals were observed in the old ice tunnel, and the possible interpretation has been discussed (Roethlisberger 1959, p. 10, Fig. 10). A new attempt has been made to determine the ice thickness by a refraction profile along the tunnel axis. The travel-time data are presented in Appendix C. As the tunnel, and thus the profile, is of limited extent, the result is questionable. The time-distance curve revealed nothing but ice overlying a refractor with a velocity of about 19000 ft/sec. Ice alone, or ice and a thin layer of till over bedrock, could explain the findings, but a V-shaped, ice-filled trough in till would also provide the same time-distance curves. Nevertheless the ice thickness can be stated to be from 100 to 170 ft at the center, 70 to 170 ft at the portal and 70 to 150 ft at the end of the tunnel.

Later seismic events

A number of later events are plotted in the time-distance graphs of refraction soundings at S1, S2 and S3 (Fig. 4, 6, 7). Such later events were very distinctive in a variety of cases, probably due to the high-frequency response of the equipment (70-425 cps filters) and to a particularity of wave propagation in frozen ground. The most spectacular records were obtained on the ice cap at location S3 (edge of ice cap), as seen in Figures 10 and 13 (Records #150858-13 and 150858-9, see App. C). In Figure 10 a strong charge (10 lb military explosive Composition C-4) brings out the refracted event related to the top of the till as first arrival and the one related to the bedrock as second event. With a small charge (1/2 - 3/4 lb 60% dynamite) only the latter is visible, followed by the direct wave as a distinct third event. Still later events are produced by special types of waves confined to the ice body, traveling part

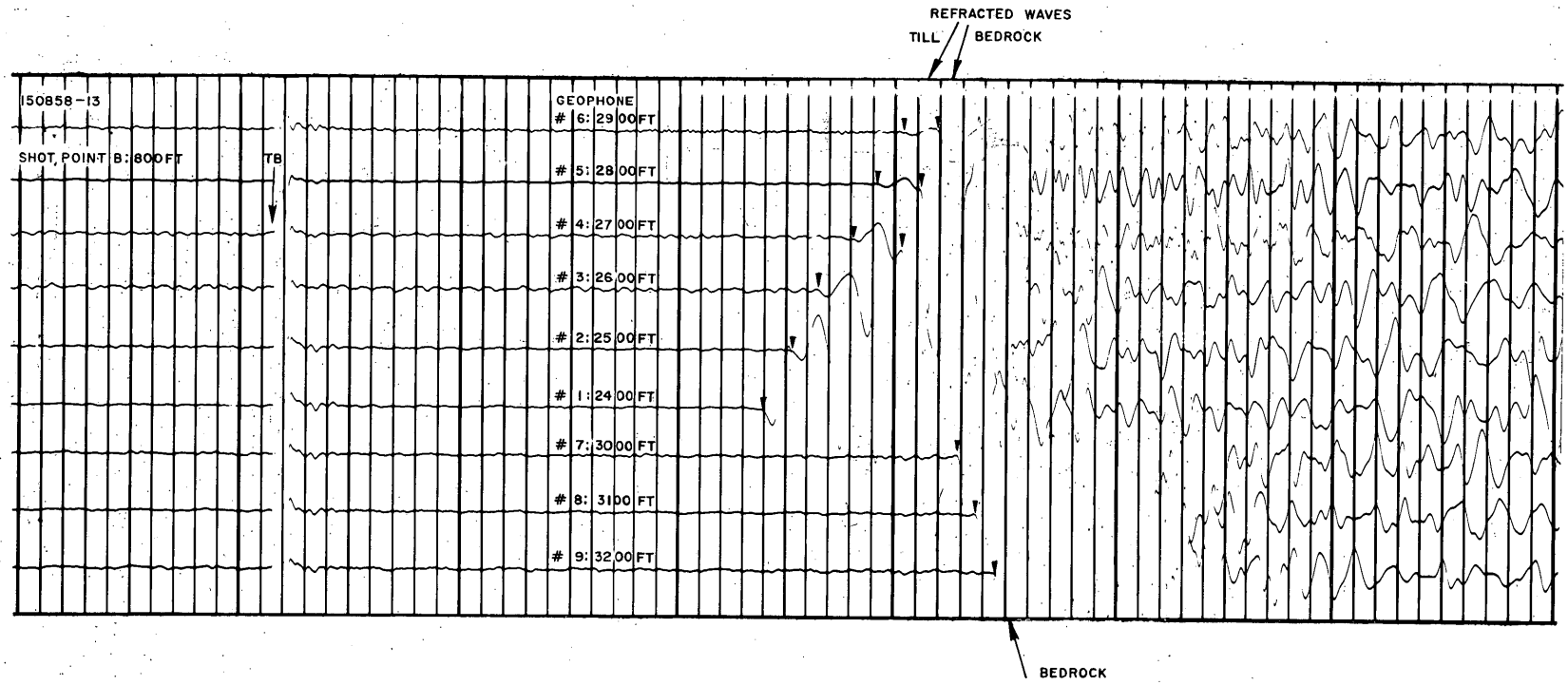

Figure 10. Heavy charge seismic record from the survey near the edge of the ice cap at S3. Time lines in 5 millisec intervals. (record #150858-13).

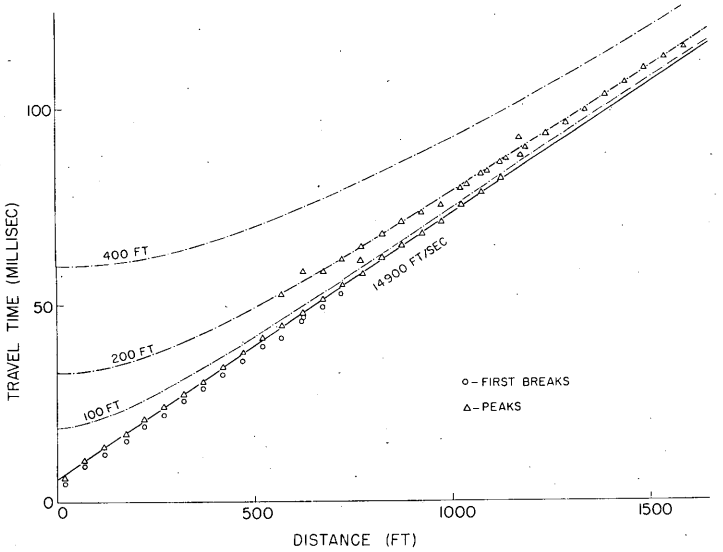

Figure 11. Time-distance curves from a profile in floodplain at S5. Theoretical curves for the first peaks of reflections from 100, 200 and 400 ft are compared with the measured values.

of their path as shear waves (reflected SP- or PS- waves and internally refracted SPS- waves).

The first and later arrivals were identified as to wave type relationship on the time-distance graph. When inspecting the records again after identification it was learned that the different events are characterized not only by their travel times, but also by the frequency and amplitude on the record. Figures 10 and 13 are very typical in this respect. The waves confined to the ice show high frequencies in the order of 400 to 500 cps and large amplitudes. The refracted wave related to the top of the bedrock shows frequencies between 200 and 300 cps and lesser amplitudes. The refracted wave related to the top of the till is typified by a very rapid decrease of amplitude with distance; the frequencies are low, 100 to 200 cps, and decrease somewhat with distance. A similar behavior was found when no ice was present at the top, and the differences in the signals of the direct and refracted wave helped considerably in identifying the high-velocity refractor in the profiles at S1 and S2.

Shallow reflection with refraction technique

Although it was not expected that a refraction survey in the floodplain halfway between Thule and TUTO (S5) would be successful, a 1600 ft profile was investigated. In that area a drill hole had been sunk to 253 ft in 1951. The drill log reported 203 ft of gravel and sand over shale, all frozen except for the active layer at the surface, which will be neglected in the following discussion. The top layer shows a higher velocity than the bottom layer according to the velocity tables. A regular refracted wave being absent, it was hoped to find later events due to PS-, SP- or SPS- waves confined to the top layer, similar to the case in which the top layer is ice. Figure 11 gives the time-distance curve of the survey. The amplitude of the first arrival typically decreased with distance as in the refraction profiles on frozen ground in the vicinity of TUTO. First breaks could only be used to a distance of about 700 ft and first arrival peaks to about 1100 ft. A much stronger onset could be traced at greater distances, lining up with a distinctive second event at distances between about 600 and 1100 ft. Figure 12 (Record #190859-10) illustrates the first and second events at these distances. The second event can be attributed to a reflected wave from the top of the low-velocity shale at a depth of approximately 200 ft. Theoretical hyperbolas for depths of 100, 200 and 400 ft are plotted in Figure 11. The drill log indicated the presence of a clay layer at the top of the shale, which may make the reflection boundary more pronounced. Strong wide-angle reflections have been reported from deep soundings and their importance for oil exploration has recently been shown by Richards (1960).

The rapid disappearance of the direct wave can readily be explained by a temperature increase with depth, causing a negative velocity gradient. The resulting curvature of the rays (concave downward) means that energy is carried away from the surface. A negative velocity gradient with depth is probably unique for permafrost and is the reason for the applicability of special methods on a small scale, as in the case of reflection soundings. The same mechanism has permitted the use of the many later arrivals in the analysis of refraction soundings. Riznichenko (1942)

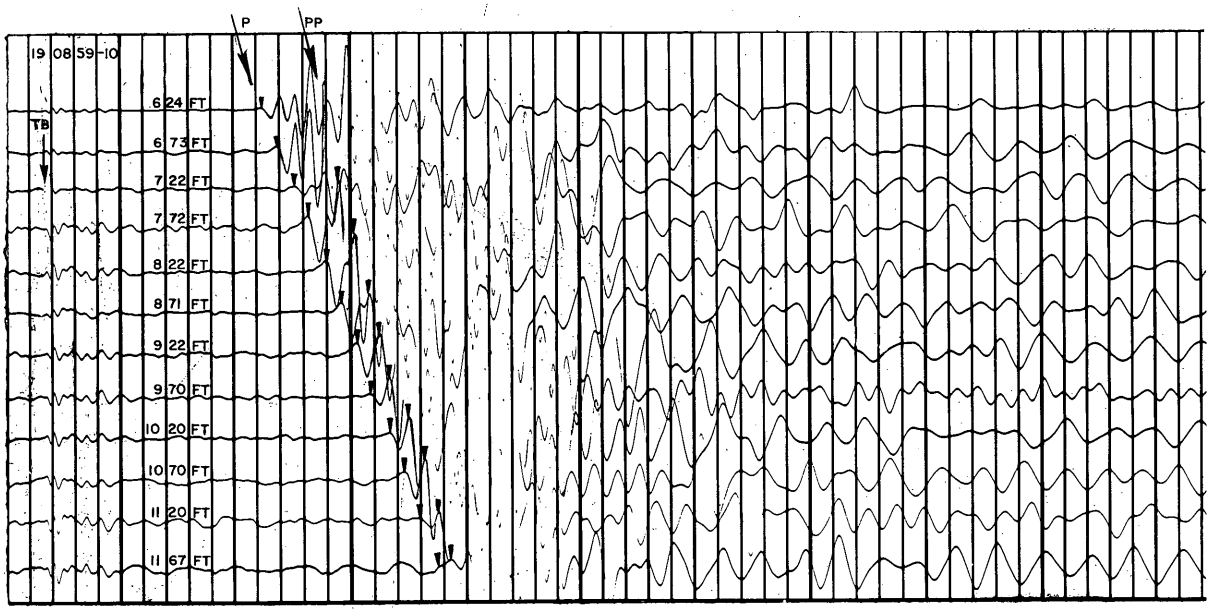

Figure 12. One of the records from which the travel times plotted in Figure 11 were derived. Time lines in 5 millisec intervals. (Record #190859-10).

has discussed the disappearance of the direct wave in more detail, taking into account the positive velocity gradient in a shallow zone close to the surface. He did not, however, stress the beneficial effect on wide angle reflection and on refraction soundings.

Glacial history

The results of the soundings in the vicinity of TUTO may have some bearing on the glacial history of a larger area. In particular the presence of some 400 ft of glacial deposit below the surface of the TUTO terrace, which forms the top of a hill, presents a problem. It is hard to believe that it could have been deposited by the local glacier, and the ice cap in the immediate vicinity of TUTO is a local glacier. It seems much more likely that the thick layer of till, probably mixed with outwash in places, was deposited alongside and close to the end of a lobe of Moltke Glacier extending south towards Petowik Glacier between TUTO and Mount Peder Marcus (P-Mountain). This would have taken place at a time when Wolstenholme Fjord was still filled with ice and Petowik Glacier and the local ice caps had retreated to a lesser extent than at present. This concept is in discord with the ideas expressed by Krinsley (Davies et al., in press). In addition to providing an explanation for the thick layer of glacial drift at TUTO, a southern lobe of the Moltke Glacier would have been a source for the melt water which carved the deep gorges in the northern part of the Petowik drainage area, including the valleys southeast of TUTO which are buried under the present ice cap (Barnes and Taylor, 1956). At the end of the ice age, local mountain glaciers, to which category the TUTO ice cap and Petowik Glacier belong, generally retreated faster than the outlet glaciers from the continental ice sheets. Although Moltke Glacier itself is probably no true outlet glacier from the inland ice, there is no doubt that it is in closer contact with it and is fed from a considerably larger and higher accumulation area than the Petowik Glacier.

CONCLUSIONS

Although the principles of seismic methods are the same as in unfrozen ground, permafrost has special properties that are important for shallow soundings. These special properties are high velocities and relatively small velocity discrimination, but velocities which are probably more homogeneous in most frozen formations than in similar unfrozen ones. Debris cemented by ice occasionally has higher velocities than consolidated rock.

In material containing clay minerals, the velocity is believed to decrease with depth because of the increasing temperature, causing the energy of the direct wave along the surface to diminish rapidly with distance. The later refracted and reflected events stand out spectacularly against the weak direct wave, as rarely experienced in a temperate climate.

In the Thule area, where the mean ground temperature is slightly below -10C, the refraction technique proved successful in most cases where shallow ice overlies frozen ground, or frozen ground overlies bedrock with or without ice on top. Where the frozen ground overlies lower velocity shale, a flat incidence (wide angle) reflection technique could be used. In order to draw conclusions on the applicability of the method in other areas, more should be known of the effect of temperature on velocity in frozen ground, and of velocities in different types of permafrost in general.

REFERENCES

Barnes, D. F., and Taylor, L. D. (1956) Gravity survey of part of the Greenland Ice Cap near Thule, U. S. Department of the Interior, Geological Survey. (unpublished ms.).

Corte, A. E. (in preparation) Relationship between four ground patterns, structure of the active layer, and type and distribution of ice in the permafrost. U. S. Army Cold Regions Research and Engineering Laboratory, Corps of Engineers, Research Report 88.

Davies, W. E.; Krinsley, D. B.; and Nicol, A. H. (in press) Geology of the North Bugt Area, northwest Greenland, Meddelelser om Grønland.

Hagedoorn, J. G. (1959) The plus-minus method of interpreting seismic refraction sections, Geophysical Prospecting, vol. 7, no. 2, p. 158-182.

Hvorslev, M. J., and Goode, T. B. (1960) Core drilling in frozen ground. Waterways Experiment Station, U. S. Army Cold Regions Research and Engineering Laboratory, Technical Report no. 3-534.

Joesting, H. R. (1954) Geophysical exploration in Alaska, Arctic, vol 7, no. 3, 4, p. 165-175.

Linehan, D. (1951) Seismology applied to shallow zone research, Symposium on surface and subsurface reconnaissance. American Society for Testing Materials, Special Technical Publication no. 122, p. 156-170.

Richards, T. C. (1960) Wide angle reflections and their application to finding limestone structures in the foothills of western Canada, Geophysics, vol. 25, no. 2, p. 385-407.

Riznichenko, V. (1942) Seismic properties of permafrost. Izvestiia Akademii Nauk SSSR, Seriia Geograficheskaia i Geofizicheskaia, vol. 6, p. 263-274.

Roethlisberger, H. (1959) Seismic survey 1957, Thule area, Greenland. U. S. Army Snow Ice and Permafrost Research Establishment, Corps of Engineers, Technical Report 64.

_____ (1961) Seismic refraction soundings in permafrost near Thule, Greenland, Proceedings, First International Symposium on Arctic Geology, Calgary 1960.

Thornburgh, H. R. (1930) Wave-front diagrams in seismic interpretation, Bulletin, American Association of Petroleum Geologists, vol. 14, no. 2.

APPENDIX A: VELOCITY MEASUREMENTS

[In each block, the first two lines give the geophone-shot point arrangement; the following lines give the record no., signal type (B = Break; P = Peak), regression no. (in parentheses), and travel times in milliseconds.]

V-1 Basement rock: gneiss (rock slab), 8 Aug 1958

Shot point and geophone	SP-W	1	2	3	4	5	6	7	8	9
Distance (feet)	0	4	50	100	150	200	250	300	350	400
080858-10 B (42)	-	1.3	-	4.2	6.7	9.0	11.7	14.9	17.4	18.4

V-1 Basement rock: gneiss (thin moraine cover), 8 Aug 1958

Shot point and geophone	SP-W	1	2	3	4	5	6	7	8	9
Distance (feet)	-10	0	50	100	150	200	250	300	350	400
080858-12 P (45)	0*	5.1*	10.7	11.9	14.0	17.5	20.3	23.5	25.2	27.8
Shot point and geophone	SP-E	9	8	7	6	5	4	3	2	1
Distance (feet)	-10	0	50	100	150	200	250	300	350	400
080858-11 B (43)	0*	3.0	5.6	7.7	10.0	12.8	15.6	17.6	20.0	23.0
080858-11 P (44)	0*	-	7.4	10.4	12.6	15.8	18.7	20.3	23.4	25.8

V-2 Wolstenholme: quartzite (thin cover of disintegrated bedrock), 21 Aug 1959

Shot point and geophone	SP-SE	1	2	3	4	5	6	7	8	9	10	11	12
Distance (meters)	-24.1	0	13.98	29.2	43.75	58.8	74.12	88.45	104.05	119	134.3	149.16	164.22
210859-2 B (34)	0*	5.5*	11.2*	14.4	16.9	19.4	21.9	24.7	27.5	30.4	32.0	35.4	38.6
210859-3 B (34)	0*	8.3*	11.5*	14.6	17.3	19.7	22.1	24.9	27.8	30.7	32.3	35.7	39.1
Shot point and geophone	SP-NW	12	11	10	9	8	7	6	5	4	3	2	1
Distance (meters)	-26.8	0	15.06	29.92	45.22	60.17	75.77	90.1	105.42	120.47	135.02	150.24	164.22
210859-5 B (35)	0*	10.0	11.9	13.8	17.6	20.0	22.6	25.0	28.1	30.7	33.2	35.8	37.6
Shot point and geophone	SP-NW	12	11	10	9	8	7	6	5	4	3	2	1
Distance (meters)	-155.5	0	15.06	29.92	45.22	60.17	75.77	90.10	105.42	120.47	135.02	150.24	164.22
210859-8 B (36)	0*	39.0	40.9	42.6	46.1	48.4	50.1	53.4	56.7	59.1	61.6	63.1	66.3

V-3 Dundas: black shale (thin cover of disintegrated bedrock mixed with moraine), 17-18 Aug 1959

Shot point and geophone	SP-E	1	2	3	4	5	6	7	8	9	10	11	12
Distance (meters)	-6.1	0	15.13	30.18	45.34	60.55	75.73	90.9	106.12	121.2	136.35	151.6	166.67
180859-1 B (11)	0*	11.9	15.2	19.0	20.9	26.5	30.1	33.3	37.7	40.9	44.9	-	-
170859-1 B (12)	0*	-	0.8	5.0	7.5	13.2	16.7	20.8	24.2	28.3	31.7	-	40.0
170859-1 P (13)	0*	-	3.3	8.1	10.0	15.8	19.1	23.3	26.7	30.7	34.9	-	43.2

* Not used for regression computation.

APPENDIX A: VELOCITY MEASUREMENTS (cont'd)

V-3 Dundas: black shale (thin cover of disintegrated bedrock mixed with moraine), 18 Aug 1959

Shot point and geophone	SP-W	12	11	10	9	8	7	6	5	4	3	2	1
Distance (meters)	-60	0	15.07	30.32	45.47	60.55	75.77	90.94	106.12	121.33	136.49	151.54	166.67
180859-2 B (17)	0*	26.7	-	-	-	-	44.2	48.2	50.9	52.5	57.5	60.8	66.7
180859-2 P (18)	0*	29.4	30.7	-	-	-	46.4	50.9	54.2	55.9	60.9	63.8	69.2
180859-3 B (14, 17)	0*	24.3	26.5	30.8	35.5	38.5	42.3	47.0	50.5	51.8	56.9	60.5	65.5
180859-3 P (15, 18)	0*	27.3	29.3	33.9	37.3	41.1	44.6	48.9	52.2	54.2	59.3	61.9	67.7
180859-4 B (16, 17)	0*	23.7	25.8	30.7	33.5	37.5	40.0	44.8	47.5	50.0	55.0	58.4	63.5
180859-4 P (18)	0*	-	-	32.6	36.2	39.8	43.3	47.6	50.8	52.7	57.7	60.3	65.8

V-3 Dundas: gray sandy shale (thin cover of disintegrated bedrock mixed with moraine), 18 Aug 1959

Shot point and geophone	SP-W	12	11	10	9	8	7	6	5	4	3	2	1
Distance (meters)	-43.6	0	15.27	30.45	45.5	60.78	76.01	91.19	106.23	121.46	136.57	151.65	166.63
180859-8 B (19)	0*	1.6	5.0	8.5	10.4	15.0	19.1	20.8	24.8	29.9	35.0	38.3	40.8
180859-8 P (20)	0*	3.4	8.0	11.0	14.0	17.9	21.9	24.1	27.3	32.2	-	-	-

V-4 Narssârssuk: dolomite (thin moraine cover), 7 Aug 1958

Shot point and geophone	SP-N	1	2	3	4	5	6	7	8	9
Distance (feet)	-10	0	50	100	150	200	250	350	450	550
070858-9 B (5)	0*	6.4*	10.5	12.9	15.9	17.7	21.2	25.4	31.4	37.0
070858-9 P (6)	0*	7.3*	11.7	14.3	16.8	18.8	22.3	26.5	32.9	-

Shot point and geophone	SP-S	9	8	7	6	5	4	3	2	1
Distance (feet)	-10	0	100	200	300	350	400	450	500	550
070858-4 B (3)	0*	6.3*	-	17.8	22.6	25.2	-	30.4	32.2	36.0
070858-5 B (3)	0*	5.8*	12.4	17.3	22.4	25.0	-	30.5	33.3	35.0
070858-4 P (4)	0*	7.1*	-	19.3	24.5	27.3	-	31.6	34.7	36.6
070858-5 P (4)	0*	- *	13.3	18.4	23.7	26.4	28.8	31.4	34.1	35.7

V-5 Narssârssuk: red sandstone (thin moraine cover), 9 Aug 1958

Shot point and geophone	SP-W	1	2	3	4	5	6	7	8	9
Distance (feet)	-10	0	50	100	150	200	250	300	350	400
090858-1 B (37, 37.1)	0*	6.3	9.2	13.5	16.7	19.9	22.6	25.0	28.8	30.7
090858-1 P (38, 38.1)	0*	-	12.7	16.4	19.7	23.8	25.5	27.6	32.2	33.6
090858-2 B (37.1)	0*	4.6	8.8	12.4	15.4	19.8	23.0	25.4	28.4	30.9
090858-2 P (38.1)	0*	-	10.2	13.6	16.8	20.7	-	-	29.2	-

Shot point and geophone	SP-W	1	2	3	4	5	6	7	8	9
Distance (feet)	-20	0	50	100	150	200	250	300	350	400
090859-3 B (39)	0*	7.1	8.3	11.7	14.2	18.2	20.0	22.5	26.7	28.4

* Not used for regression computation.

V-5 Narssârssuk: red sandstone (thin moraine cover), 9 Aug 1958

Shot point and geophone	SP-E	9	8	7	6	5	4	3	2	1
Distance (feet)	-25	0	50	100	150	200	250	300	350	400
090859-5 B (40)	0*	7.9	12.5	14.3	18.0	19.5	23.7	27.8	28.3	31.9
090859-5 P (41)	0*	9.2	14.4	16.5	19.8	23.3	25.8	28.7	30.9	34.1

V-6 Dike: diabase (disintegrated bedrock mixed with moraine), 9 Aug 1958

Shot point and geophone	SP-N	1	2	3	4	5	6	7	8	9
Distance (feet)	-20	0	50	100	150	200	250	300	350	400
090858-8 B (7)	0*	5.9	8.0	10.6	12.9	15.1	18.9	21.9	23.3	27.1
090858-8 P (8)	0*	-	9.6	12.5	15.0	18.2	20.8	24.2	25.7	29.4

Shot point and geophone	SP-S	9	8	7	6	5	4	3	2	1
Distance (feet)	-10	0	50	100	150	200	250	300	350	400
090858-9 B (9)	0*	3.9	6.8	9.8	13.0	15.5	17.6	21.4	23.8	26.5
090858-9 P (10)	0*	-	9.0	12.3	14.9	17.7	19.8	23.2	25.8	28.8

S-1 Glacial deposit: till (permafrost tunnel), 28 Aug 1959

Shot point and geophone	SP-S	1	2	3	4	5	6	7	8	9	10	11
Distance (feet)	-4	0	20	40	60	80	100	120	140	160	180	200
280859-2 B (21)	-	0	1.29	2.78	3.76	5.09	6.21	7.61	-	10.13	11.79	12.71
280859-5 B (21)	-	0	1.23	2.26	4.15	5.21	6.61	7.68	9.24	10.24	11.86	12.85
280859-6 P(S') (22)	-	-	-	8.3	10.4	13.0	14.8	18.1	20.7	23.5	-	-
280859-7 P(S') (23)	-	4.0	5.1	-	10.1	12.5	14.4	17.8	20.1	22.8	24.6	26.8

Shot point and geophone	SP-N	11	10	9	8	7	6	5	4	3	2	1
Distance (feet)	-4	0	20	40	60	80	100	120	140	160	180	200
280859-12 B (24)	-	0	-	2.9	4.4	5.8	7.1	8.4	9.3	10.7	11.7	13.3

S-5 Glacial deposit: outwash (flooded cobble field), 19, 20 Aug 1959

Shot point and geophone	SP-N	1	2	3	4	5	6	7	8	9	10	11	12
Distance (meters)	-6.1	0	15.01	29.97	45.09	60.4	75.34	90.7	105.65	120.73	136.0	151.3	165.65
190859-5 B (25)	0*	4.7	9.3	12.3	15.5	19.6	22.2	25.7	28.7	-	35.7	39.4	-
190859-5 P (26)	0*	6.1	10.8	14.1	17.3	21.1	24.1	27.3	30.1	-	37.8	41.5	-

Shot point and geophone	SP-N	1	2	3	4	5	6	7	8	9	10	11	12
Distance (meters)	-67.0	0	15.01	29.97	45.09	60.4	75.34	90.7	105.65	120.73	136.0	151.3	165.65
190859-9 B (27)	0*	18.7	21.5	25.0	23.8	31.7	35.0	38.3	40.8	45.0	48.1	52.8	58.8
190859-9 P (28)	0*	20.3	23.8	27.0	30.6	34.1	37.2	40.3	44.0	47.4	50.8	54.3	61.0

* Not used for regression computation.

S-5 Glacial deposit: outwash (flooded cobble field), 19, 20 Aug 1959

Shot point and geophone	SP-N	1	2	3	4	5	6	7	8	9	10	11	12
Distance (meters)	-190.4	0	15.01	29.97	45.09	60.4	75.34	90.7	105.65	120.73	136.0	151.3	165.65
190859-10 P (29)	0*	47.7	51.4	55.1	57.8	61.7	64.9	67.9	70.8	75.0	78.2	81.6	-
Shot point and geophone	SP-S	12	11	10	9	8	7	6	5	4	3	2	1
Distance (meters)	-101.0	0	14.35	29.65	44.92	60.0	74.95	90.31	105.25	120.56	135.68	150.64	165.65
200859-5 B (32)	0*	24.2	27.7	30.2	33.5	36.6	39.4	42.9	46.1	50.7	53.2	56.2	59.5
200859-5 P (33)	0*	26.1	29.4	32.9	35.8	38.1	41.8	45.4	48.9	52.4	55.4	58.6	61.7

Petowik Glacier: glacier ice (bare ice), 24 Aug 1959

Shot point and geophone	SP-E	1	2	3	4	5	6	7	8	9	10	11	12
Distance (feet)	-486.0	0	122.0	249.0	376.0	502.5	629.8	756.1	883.0	1009.5	1136.5	1263.0	1388.3
240859-2 B (0, 1)	0*	43.0	52.4	57.5	72.9	83.0	93.5	104.2	114.3	124.6	135.2	145.2	155.5
240859-3 B (2, 1)	0*	42.2	52.3	62.3	73.5	83.5	93.9	103.9	114.0	124.1	134.6	144.8	155.0

* Not used for regression computation.

APPENDIX B. Differences Δ between travel times.

V-1 Basement rock: gneiss, 8 Aug 1958

Shot point and geophone no.	Distance (m)	Distance (ft)	Record no. / Signal type / Regression no.	Travel time (millisec) 080858-11 Peak	080858-12 Peak	Δ 111
1		0		-	27.8	-
2		50		7.4	25.2	-17.8
3		100		10.4	23.5	-13.1
4		150		12.6	20.3	-7.7
5		200		15.8	17.5	-1.7
6		250		18.7	14.0	4.7
7		300		20.3	11.9	8.4
8		350		23.4	10.7	12.7
9		400		25.8	-	-

V-2 Wolstenholme, Quartzite, 21 Aug 1959

		Record no. / Signal type / Regression no.	210859-3 Break	210859-5 Break	103
1	0		8.3	37.6	-29.3
2	13.98		11.5	35.8	-24.3
3	29.20		14.6	33.2	-18.6
4	43.75		17.3	30.7	-13.4
5	58.80		19.7	28.1	-8.4
6	74.12		22.1	25.0	-2.9
7	88.45		24.9	22.6	2.3
8	104.05		27.8	20.0	7.8
9	119.00		30.7	17.6	13.1
10	134.30		32.3	13.8	18.5
11	149.16		35.7	11.9	23.8
12	164.22		39.1	10.0	29.1

V-3 Dundas, black shale, 17, 18 Aug 1959

		Record no. / Signal type / Regression no.	170859-1 Break	180859-3 Break	106
1	0		-	-	-
2	15.13		0.8	60.5	-59.7
3	30.18		5.0	56.9	-51.9
4	45.34		7.5	51.8	-44.3
5	60.55		13.2	50.5	-37.3
6	75.73		16.7	47.0	-30.3
7	90.90		20.8	42.3	-21.5
8	106.12		24.2	38.5	-14.3
9	121.20		28.3	35.5	-7.2
10	136.35		31.7	30.8	0.9
11	151.60		-	26.5	-
12	166.67		40.0	24.3	15.7

V-3 Dundas: black shale, 17, 18 Aug 1959 (cont'd)

Shot point and geophone no.	Distance (m)	Distance (ft)	Record no. / Signal type / Regression no.	Travel time (millisec) 170859-1 Peak	Travel time (millisec) 180859-3 Peak	Δ 107
1	0			-	-	-
2	15.13			3.3	61.9	-58.6
3	30.18			8.1	59.3	-51.2
4	45.34			10.0	54.2	-44.2
5	60.55			15.8	52.2	-36.4
6	75.73			19.1	48.9	-29.8
7	90.90			23.3	44.6	-21.3
8	106.12			26.7	41.1	-14.4
9	121.20			30.7	37.3	-6.6
10	136.35			34.9	33.9	1.0
11	151.60			-	29.3	-
12	166.67			43.2	27.3	15.9

V-4 Narssârssuk: Dolomite, 7 Aug 1958

			Record no. / Signal type / Regression no.	070858-9 Break	070858-5 Break	101
2	50			10.5	33.3	-22.8
3	100			12.9	30.5	-17.6
4	150			15.9	-	-
5	200			17.7	25.0	-7.3
6	250			21.2	22.4	-1.2
7	350			25.4	17.3	8.1
8	450			31.4	12.4	19.0
			Record no. / Signal type / Regression no.	070858-9 Peak	070858-5 Peak	102
2	50			11.7	34.1	-22.4
3	100			14.3	31.4	-17.1
4	150			16.8	28.8	-12.0
5	200			18.8	26.4	-7.6
6	250			22.3	23.7	-1.4
7	350			26.5	18.4	8.1
8	450			32.9	13.3	19.6

V-5 Narssârssuk: Red sandstone, 9 Aug 1958

			Record no. / Signal type / Regression no.	090858-3 Break	090858-5 Break	110
1	0			7.1	31.9	-24.8
2	50			8.3	28.3	-20.0
3	100			11.7	27.8	-16.1
4	150			14.2	23.7	-9.5
5	200			18.2	19.5	-1.3
6	250			20.0	18.0	2.0
7	300			22.5	14.3	8.7
8	350			26.7	12.5	14.2
9	400			28.4	7.9	20.5

GPO 813780—5

V-6 Dike: Diabase, 9 Aug 1958

Shot point and geophone no.	Distance (m)	Distance (ft)		Travel time (millisec) 090858-8 Break	090858-9 Break	Δ
			Record no. / Signal type / Regression no.			104
1		0		5.9	26.5	-20.6
2		50		8.0	23.8	-15.8
3		100		10.6	21.4	-10.8
4		150		12.9	17.6	-4.7
5		200		15.1	15.5	-0.4
6		250		18.9	13.0	5.9
7		300		21.9	9.8	12.1
8		350		23.3	6.8	16.5
9		400		27.1	3.9	23.2
			Record no. / Signal type / Regression no.	090858-8 Peak	090858-9 Peak	105
1		0		-	28.8	-
2		50		9.6	25.8	-16.2
3		100		12.5	23.2	-10.7
4		150		15.0	19.8	-4.8
5		200		18.2	17.7	0.5
6		250		20.8	14.9	5.9
7		300		24.2	12.3	11.9
8		350		25.7	9.0	16.7
9		400		29.4	-	-

S-5 Glacial deposit: Outwash, 19,20 Aug 1959

				190859-9 Break	200859-5 Break	
			Record no. / Signal type / Regression no.			108
1	0			18.7	59.5	-40.8
2	15.01			21.5	56.2	-34.7
3	29.97			25.0	53.2	-28.2
4	45.09			28.3	50.7	-22.4
5	60.40			31.7	46.1	-14.4
6	75.34			35.0	42.9	-7.9
7	90.70			38.3	39.4	-1.1
8	105.65			40.8	36.6	4.2
9	120.73			45.0	33.5	11.5
10	136.00			48.1	30.2	17.9
11	151.30			52.8	27.7	25.1
12	165.65			58.8	24.2	34.6
			Record no. / Signal type / Regression no.	190859-9 Peak	200859-5 Peak	109
1	0			20.3	61.7	-41.4
2	15.01			23.8	58.6	-34.8
3	29.97			27.0	55.4	-28.4
4	45.09			30.6	52.4	-21.8
5	60.40			34.1	48.9	-14.8
6	75.34			37.2	45.4	-8.2
7	90.70			40.3	41.8	-1.5
8	105.65			44.0	38.1	5.9
9	120.73			47.4	35.8	11.6
10	136.00			50.8	32.9	17.9
11	151.30			54.3	29.4	24.9
12	165.65			61.0	26.1	34.9

APPENDIX C: Travel time (refraction soundings).

S 1

Record no.	250758-1	250758-2	250758-3
Shot point location (ft)	490	490	710
Geophone location (ft)	Travel time (millisec)		
700	28.0	19.1	6.5
675	26.4	17.9	8.3
650	25.0	15.9	9.8
625	23.2	14.0	11.6
600	20.7	11.5	12.4
575	20.0	11.2	15.3
550	18.3	9.4	17.1
525	16.9	8.0	18.6
500	15.0	6.2	19.8
Remarks	Wrong type of cap		

Record no.	250758-4	250758-5	250758-6		250758-7	250758-8	
Shot point location (ft)	910	490	1300		1300	1700	
Geophone location (ft)			Travel time (millisec)				
900	5.8	33.2	31.3		30.4	58.3	
850	8.5	28.4	33.3		32.4	60.4	
800	12.3	25.2	36.7		35.7	63.6	
750	16.5	22.6	40.7		39.8	67.5	
700	20.1	18.5	43.8		43.9	71.4	90.0
650	23.4	15.2	48.3		46.5	75.2	91.8
600	26.5	11.6	50.6	54.1	49.5	78.3	93.1
550	30.6	9.2	54.0	58.3	53.2		97.2
500	32.6	5.0	56.8	60.0	55.7		98.2
Remarks							Peaks

Record no.	250758-9			250758-10	
Shot point location (ft)	1700			2100	
Geophone location (ft)	Travel time (millisec)				
900	54.7	56.6	82.4		
850	56.0	57.4	84.1		
800	59.9	61.6	88.2		
750	64.2	65.9	92.4		
700	68.1	69.4	95.7	108.2	110.9
650	70.9	72.7		110.4	113.5
600	73.5	75.2		111.7	114.5
550	78.2	79.7			118.2
500	80.9	81.8		117.4	120.0
Remarks	Breaks	Peaks	Breaks	Peaks	Peaks

APPENDIX C: (cont'd)

S 1

Record no.	250758-11		250758-12		260758-1	260758-2
Shot point location (ft)	2100		2500		410	-10
Geophone location (ft)	Travel time (millisec)					
0	138.4	141.1	158.1	160.2	32.5	6.5
50	136.1	138.4	155.8	157.2	29.9	10.8
100	133.4	135.7	152.7	155.0	26.3	13.7
150	131.1	133.4	150.5	153.3	23.5	17.5
200	127.2	129.1	148.1	150.1	18.7	20.8
250	124.2	125.9	145.6	147.8	16.0	23.5
300	119.2	121.9	144.5	145.7	12.0	27.7
350	-	-	141.1	143.1	7.8	29.9
400	112.9	115.1	138.8	141.3	5.7	33.2
Remarks	Breaks	Peaks	Breaks	Peaks		

Record no.	260758-3		260758-4		260758-5		260758-6	260758-7
Shot point location (ft)	0		600		600		2510	2090
Geophone location (ft)								
2500	157.5	159.3	130.0	131.5		130.5	1.7	37.1
2450	155.0	157.1	128.4	129.7		128.8	9.2	34.3
2400	152.5	154.8	125.0	126.7		126.8	12.5	31.0
2350	150.5	152.6	123.4	125.0		125.5	16.3	26.3
2300	-	-	118.0	123.7		122.8	22.0	23.3
2250	146.8	149.3	112.5			119.3	25.0	18.8
2200	144.7	147.6	109.5		112.3	119.2	30.0	15.6
2150	141.0	143.3	105.0		106.8	117.2	35.0	10.8
2100	139.2	141.2	101.5		102.2		-	8.0
Remarks			Breaks	Peaks	Poor record			

S 2

Record no.	050858-3	050858-4	050858-5		050858-6		050858-7
Shot point location (ft)	2328	1489	1100		700		0
Geophone location (ft)							
1500	57.3	5.6	35.1		59.0		104.2
1600	50.8	12.8	40.8		65.6		110.7
1700	43.9	19.8	47.8		71.5		116.4
1800	37.7	28.1	54.5		78.1		123.2
1900	31.3	33.3	60.9	80.3	84.3		129.7
2000	24.4	39.5	66.5	84.5	90.0		134.7
2100	18.9	46.8	73.9	92.5	97.7	108.1	140.7
2200	11.8	52.3	80.0	96.8	104.2	111.7	145.6
2300			86.2	102.1	110.7	116.7	149.8
2310	2.9	58.1					

S 3

Record no.	140858-1	140858-2	140858-7	140858-8	140858-9
Shot point location (ft)	-10	810	1600	1600	2400
Geophone location (ft)		Travel time (millisec)			
0	1.5	64.0	131.2	112.4	197.5
100	9.7	57.2	123.5	107.4	189.4
200	18.1	50.6	115.4	100.1	181.4
300	26.0	42.5		93.5	173.1
400	34.3	34.3	99.1	87.4	165.6
500	42.4	26.4	91.2	80.6	157.5
600	50.7	18.2	82.9	74.4	149.0
700	57.3	10.1	75.2	68.4	139.8
800	64.0	1.5	66.3	61.5	131.5

Record no.	140858-10			140858-12	
Shot point location (ft)	2400			3200	
Geophone location (ft)					
0		173.8		205.1	206.8
100		169.7		201.0	203.0
200		165.5	168.0	196.8	198.5
300	155.8	160.3	162.5	192.0	166.9
400	149.4	155.1	156.5	185.7	172.6
500	142.7	151.4	152.4	181.5	178.2
600	126.1 136.9	144.7	146.4	176.0	183.2
700	119.0 130.5			170.1	187.4
800	112.2 123.6			165.1	194.9
Remarks	Peak		Peak		Peak

Record no.	150858-1		150858-4		150858-6		150858-9		150858-10		
Shot point location (ft)	3210		2390		1600		800		800		
Geophone location (ft)											
2400	61.7	67.8	2.2		60.3		132.3	137.7	112.5	122.0	
2500	54.9	59.7	10.4		66.3		137.7	141.4	118.9	127.5	
2600	49.3		18.4		72.7		140.1	149.4	126.7	133.7	140.0
2700	42.9		26.4		78.8		143.5	157.5		140.0	143.7
2800	35.1		34.7		85.5		148.3	165.8			148.0
2900	26.9		41.7		91.6		152.7	173.5			151.8
3000	18.6		48.1		98.6	107.5	156.9	181.8			156.7
3100	10.6		54.1	59.4	106.4	112.6	161.0	189.3			160.6
3200	2.1		61.1	68.7	111.6	116.5	165.8	198.3			165.0

APPENDIX C: (cont'd)

S 3

Record no.	150858-11				150858-12	150858-13	
Shot point location (ft)	0				0	800	
Geophone location (ft)							
2400	175.0	-	198.0	210.6	174.1	112.3	
2500	178.3	-	205.8	219.2	177.7	118.5	
2600	-	-	214.0	-	180.8	124.7	
2700	-	-	222.3	-	184.1	133.3	144.0
2800	188.5	208.1	230.0	243.0	188.4	138.3	148.0
2900	193.0	210.8	237.7	265.2	192.8	144.5	152.0
3000	197.5	214.2	245.8	257.5	197.3		156.5
3100	200.8	218.3	254.2	278.7	201.2		160.6
3200	205.6	221.7	261.0	282.5	205.5		165.3

Record no.	160858-1			160858-2			160858-3	160858-4		
Shot point location (ft)	0			0			0	0		
Geophone location (ft)										
1050	79.8			88.1	100.9		88.0	79.6		
1250	92.7			103.6	115.5		104.0	91.8	95.1	
1450	105.6			119.1			119.8	104.5	107.2	
1600	115.7			131.8			131.7	113.2	117.1	
1700				139.6		140.8	139.7	120.0	123.2	
1800		145.2			145.3	146.9	144.9	125.5	129.5	
1900		149.3			149.6	151.4	149.4	131.2	135.3	148.6
2000		153.7			153.6	155.5	153.6	137.8	142.2	153.1
2150		-						146.4	152.0	161.2
Remarks						Peaks			Peaks	

Record no.	160858-5		160858-6		160858-7	160858-9	160858-11		
Shot point location (ft)	800		800		1600	2400	3200		
Geophone location (ft)									
1050	22.8	23.8			45.7	96.0			150.0
1250	38.8	40.0			29.9	83.0			137.0
1450	53.1	54.2			13.5	70.8		124.0	125.5
1600	62.8	63.9			2.0	61.5	112.5	114.3	116.6
1700	68.7	69.7	77.1		9.9	55.0	105.3	108.4	111.3
1800	74.3		84.7		18.0	48.9	98.5	101.7	
1900	80.1		92.9		26.1	42.5	93.2	95.4	
2000	86.2		99.9		34.6	35.2	87.2	89.6	
2150	96.2		108.2		44.8	24.0	77.0	79.5	
Remarks								Peaks	

S 3

Record no.	160858-13			
Shot point location (ft)	3200			
Geophone location (ft)				
1050	151.3	177.6	193.5	207.8
1250	137.7	161.4	-	-
1450	126.0	145.0	157.3	175.7
1600	117.5	131.8		
1700	112.4	125.2		
1800	106.8	116.8		
1900	102.7	108.5		
2000	101.5	-		
2150	-	-		

S 4

Record no.	300858-1		300858-2		300858-3			300858-4	
Shot point location (ft)	1070		1070		1070				
Geophone location (ft)									
267	-		62.8		62.5			65.7	
367	-		57.5		57.2			58.9	
467	-		50.7		50.0			50.3	52.9
567	43.4		41.4		41.4	44.1		44.1	51.0
667	36.3	40.2	33.7	45.0	33.4	36.7	44.8	36.3	44.6
767	29.2	37.2		37.8	26.3	29.1	37.4	29.2	37.8
867		35.9		35.1	18.2	23.8	34.8	23.8	
967		-	10.0		9.6	19.1			
1067		-	1.3		-	-	-		

Record no.	300858-6			300858-7			300858-8	300858-12	
Shot point location (ft)	264			264			0	67	
Geophone location (ft)									
267	1.5			1.4			22.2	-	9.5
367	-			-			31.2	-	17.5
467	18.1	34.5		18.3			39.0	34.5	25.2
567	25.4	28.9	35.9	25.6	28.1	36.5	46.5	41.5	32.8
667	33.2	37.9	45.5	33.8	37.3		54.7	49.6	40.8
767	41.4	44.8			-		60.9	57.7	48.7
867				48.4	52.3		66.2	63.0	56.4
967				58.0			71.7	68.7	62.7
1067				63.3	77.4		76.2	73.1	67.6

S 5

Record no.	190859-5		190859-9		190859-10			200859-4	200859-5	
Shot point location (ft)	-20		-220		-624			-1039	875	
Geophone location (ft)	Travel time (millisec)									
0	4.7	6.1	18.7	20.3	46.6	47.7	58.5	80.1	59.5	61.7
49.2	9.3	10.8	21.5	23.8	49.2	51.4	58.3	83.4	56.2	58.6
98.3	12.3	14.1	25.0	27.0		55.1	61.5	86.5	53.2	55.4
147.9	15.5	17.3	28.3	30.6		57.8	64.3	89.3	50.7	52.4
198.1	19.6	21.1	31.7	34.1		61.7	67.6	93.0	46.1	48.9
247.1	22.2	24.1	35.0	37.2		64.9	70.9	95.7	42.9	45.4
297.5	25.7	27.3	38.3	40.3		67.9	73.0	99.2	39.4	41.8
346.5	28.7	30.1	40.8	44.0		70.8	75.0	102.8	36.6	38.1
396.0	-	-	45.0	47.4		75.0	79.2	106.1	33.5	35.8
446.1	35.7	37.8	48.1	50.8		78.2	82.7	109.9	30.2	32.9
496.3	39.4	41.5	52.8	54.3		81.6	85.7	112.4	27.7	29.4
543.3	-	- 52.4	58.8	61.0 65.0		-	87.4 92.0	114.9	24.2	26.1
Remarks	Break	Peak	Break	Peak	Break	Peaks		Peaks	Break	Peak

GPO 813780—4

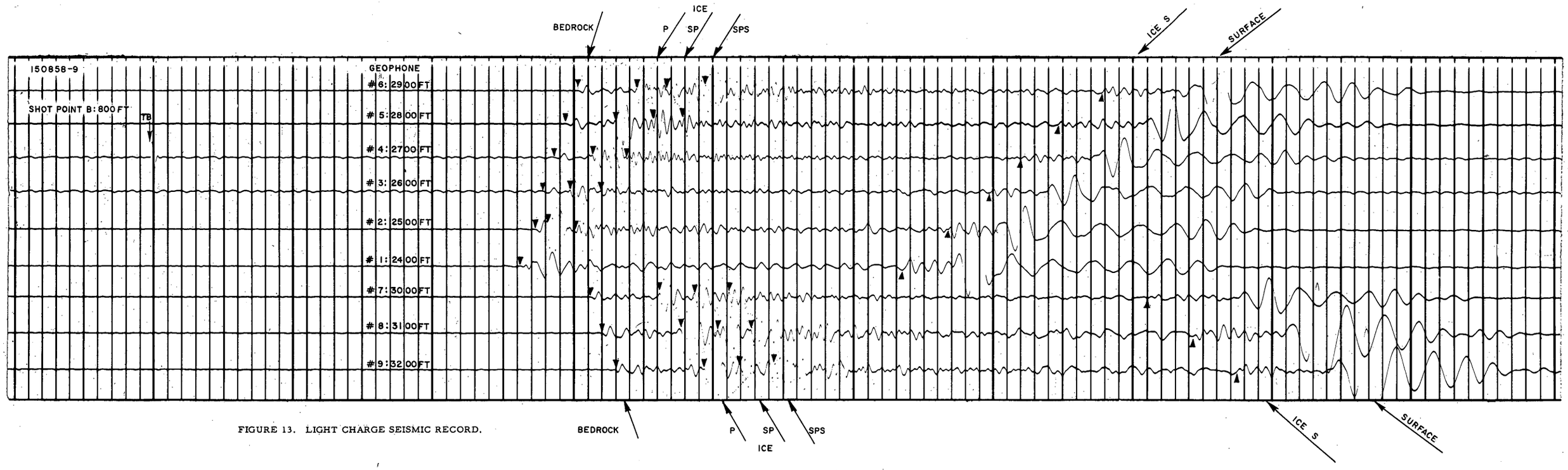

FIGURE 13. LIGHT CHARGE SEISMIC RECORD.

GPO 813780-3